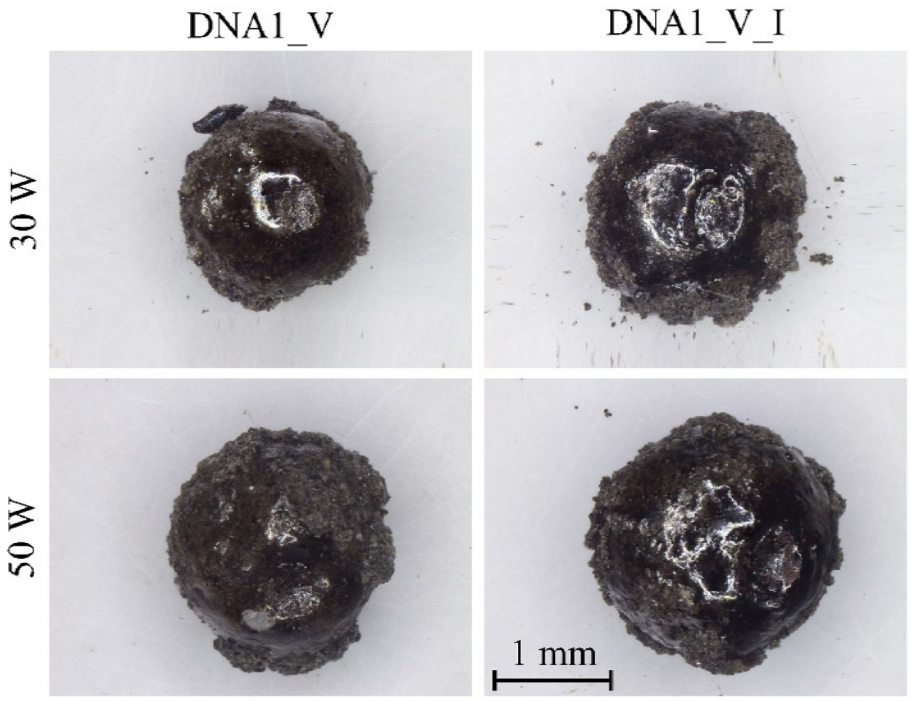

Fig. 9. Microscope images of samples obtained in vacuum.

Table 5
Detailed results of the mass and dimension of the samples obtained in vacuum.

Simulant	Sintering time [s]	Forward power [W]	Mass [mg]	Eq. diam. [mm]	Simulant	Sintering time [s]	Forward power [W]	Mass [mg]	Eq. diam. [mm]
DNA1_V	10	30	5.3	2.080	DNA1_V_I	10	30	6.5	2.520
DNA1_V	10	50	7.7	2.520	DNA1_V_I	10	50	9.2	2.850

to be in the right-hand region of the Paschen curve, while conditions from 10 mbar to 0.1 mbar could correspond to the minimum of the curve, with a high likelihood that the antenna behaviour is negatively affected by uncontrolled discharges. Below 0.05 mbar, the system regains a more stable behaviour. Although the phenomenon of discharges requires careful mitigation in the experiments, the risk is most probably self-extinguishing on the lunar surface, where pressures of $3 \bullet 10^{-12}$ mbar are far left in the Paschen's curve.

2.5. Experimental planning

The sintering tests were performed according to the planning described below.

1) Stationary tests in air at room pressure: the antenna tip was placed in a fixed position at a distance of 0.1–0.5 mm from the powder bed and the microwave generator was activated at a set power for a certain time.
2) Stationary tests in air at low pressure: the tests conducted at room pressure were repeated at a pressure of 0.01 mbar.
3) Dynamic tests at room pressure: the antenna tip was moved along a tool-path on the powder bed to obtain bigger volumes of consolidated regolith.

It was not possible to conduct dynamic tests at low pressure due to difficulties in operating the system, which will be addressed in future developments of the research.

After each test, the amount of regolith below the tip was analysed according to the following protocol:

- Check of the presence of solid agglomerates;
- Removal of loose powder from the sintered samples with a thin brush;
- Microscopic observation with a Nikon SMZ1270i stereo microscope to examine the overall appearance of the samples and measure the equivalent diameter;
- Mass measurement with an Ohaus PA124C analytical scale, with a resolution of 0.1 mg.

The equivalent diameter was calculated as the mean between the maximum and minimum Feret's diameters [38].

Owing to the phenomena of discharges described in Section 2.4, the maximum power at low pressure was limited to 50 W. The sintering time was chosen by balancing two factors: the mass of the sintered material and the heat generated during the process. Since at low pressure heat dissipation occurs only by radiation, the temperature of the critical equipment (antenna and RF cables) was carefully monitored. Thermal issues are expected to be self-extinguishing in the lunar environment, hence the study did not consider any specific cooling solution. A process time of 10 s was considered the best option to obtain a good amount of solidified material in a regular shape without raising the temperature of the critical devices above dangerous levels.

Table 3 describes the process parameters set in the sintering tests at room and low pressure.

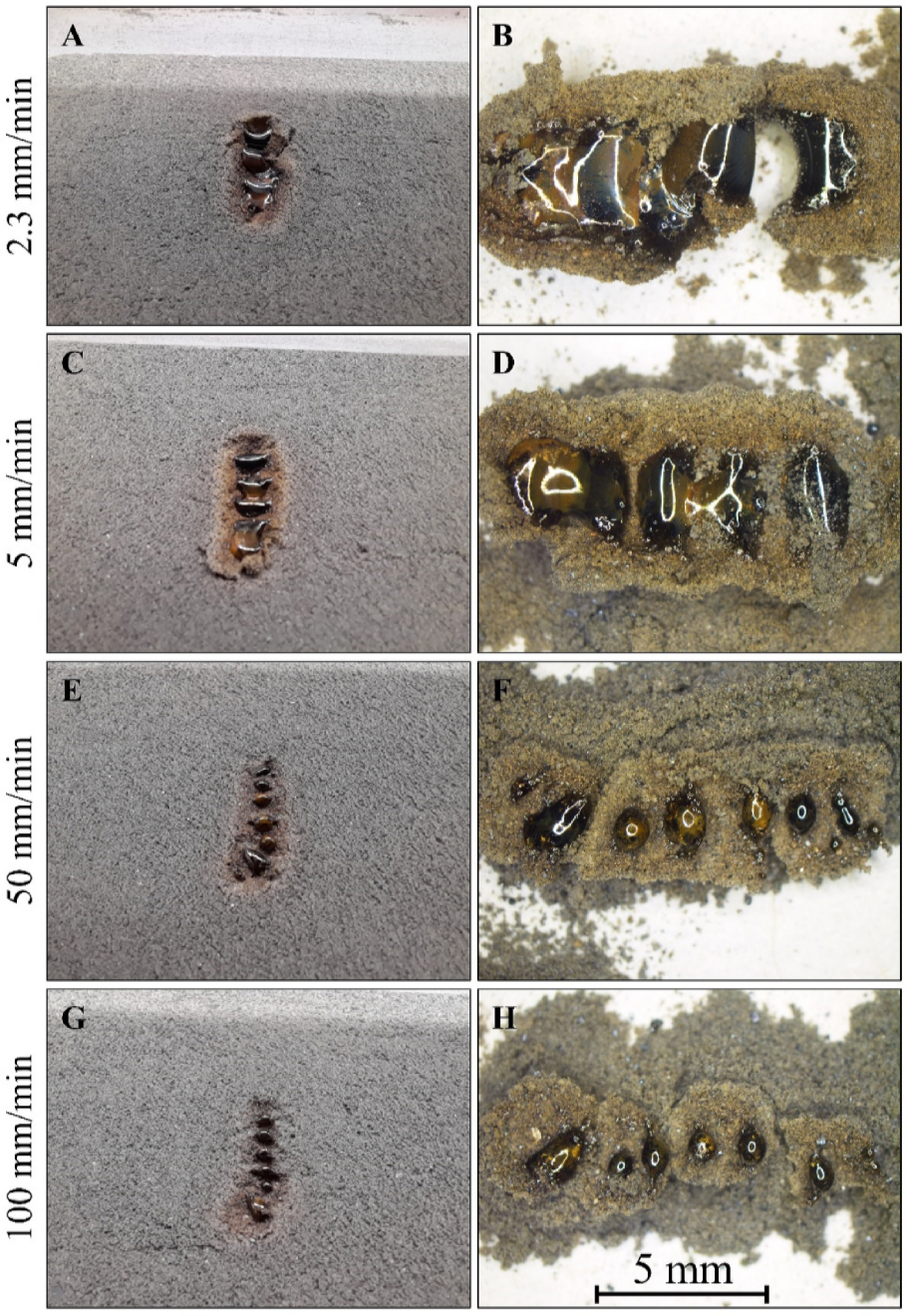

Fig. 10. Photos and microscope images of the samples obtained with various feed rates: a) and b) 2.3 mm/min, c) and d) 5 mm/min, e) and f) 50 mm/min, g) and h) 100 mm/min.

3. Results

3.1. Room pressure stationary tests

In stationary tests at room pressure, consolidated samples were successfully obtained with both simulants. Some representative microscope images of the samples are shown in Fig. 6 for DNA1_V and in Fig. 7 for DNA1_V_I. For each sintering time and simulant, 2 samples are shown, one produced at a low power (60–70 W) and one at a higher power (90–100 W). Their appearance depends mainly on the sintering time:

- A sintering time of 1 s produces irregular samples with an approximate size of 1 mm, sometimes consisting of only partially sintered material.
- Starting from a sintering time of 10 s a glassy melt is achieved, the samples increase in volume and mass and take on a regular spherical shape.
- By increasing the sintering time to 100 s, the spheres open up and a "meltpool-like" geometry is obtained.

Table 4 summarises the results of the mass and dimension measures of the molten particles obtained by stationary tests performed at room pressure on the two simulants.

The effect of forward power and sintering time on the mass of molten particles can be better appreciated in the plot of Fig. 8.

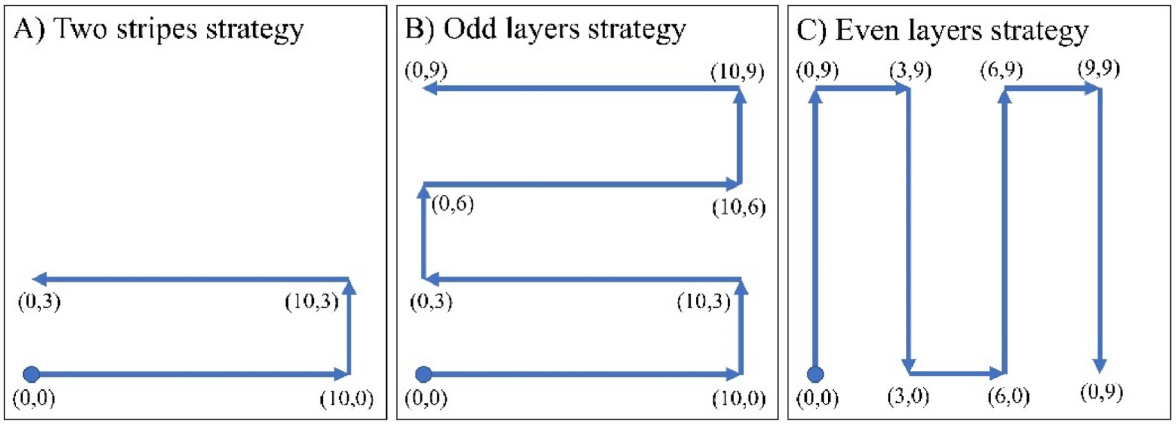

Fig. 11. Scanning strategies adopted for the multiple stripes sintering tests: a) two stripe strategy, b) odd layer strategy, c) even layer strategy.

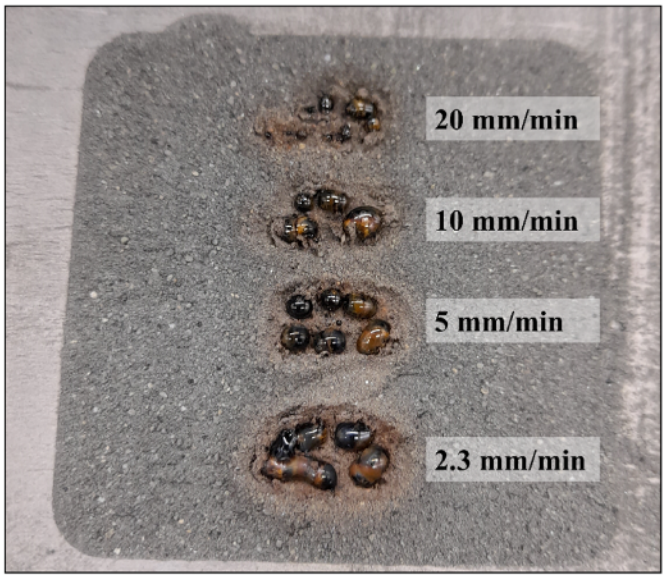

Fig. 12. Adjacent stripes produced at different feed rates.

Some considerations arise:

- The mass of the molten material increases with increasing power and time. The effect of sintering time is much more pronounced.
- The average mass of the samples is higher for DNA_1V than for DNA_1_V_I. This result refuses the expectation that the ilmenite content would have favoured the coupling with microwaves.

3.2. Stationary tests in vacuum

As planned, two power-time combinations were tested. Preliminary tests showed that the phenomenon of uncontrolled dissipative discharges is more likely to occur at high power levels. Thus, at the lowest power used in room pressure tests (60 W), the discharges already reduce the power transferred to the powder in such a way as to prevent any consolidation. On the other hand, it was found that in vacuum it was possible to achieve melting with a forward power of only 30 W. For this reason, the power values for the tests at low pressure were set at 30 W and 50 W, just below the range tested in air.

Unfortunately, due to the low power, it was not possible to consolidate the material by keeping the tip at a distance of 0.1–0.5 mm from the powder bed. Therefore, the tests were repeated with the tip protruding 0.2 mm into the powder bed. Thus, a melt was successfully obtained, but it stuck to the tip of the antenna and had to be detached before it could be analysed.

Fig. 9 shows the samples obtained in vacuum. The appearance is that of a regular sphere with a conical depression left by the antenna tip.

Details of mass and dimensions are given in Table 5. In this case, the effect of ilmenite was opposite to that observed in air, and the simulant DNA1_V_I was consolidated into larger and heavier samples.

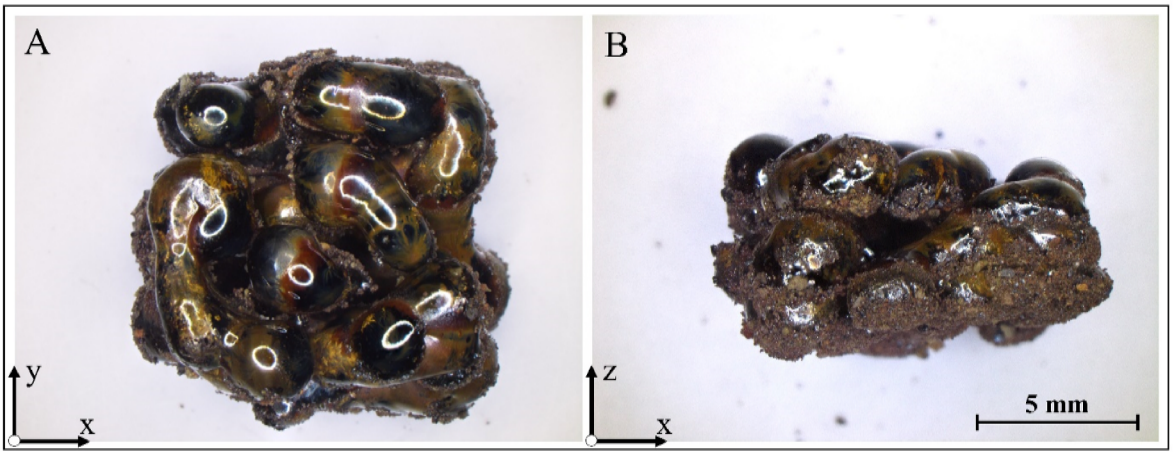

Fig. 13. Cube obtained with the superimposition of 5 layers.

3.3. Room pressure dynamic tests

In order to investigate the ability of the developed solution to produce larger solid samples by moving the tip along a pre-determined tool path composed of stripes, additional tests were conducted at room pressure in air. In this condition, the identified process window allows the use of a higher power and consequently keeping the tip at a distance from the powder bed so that no adhesion of the material to the tip occurs. The purpose of these tests was to determine the feasibility of operating the localized microwaves as a CNC tool, once the adhesion problems were solved. As mentioned earlier, the discharge phenomena that limit the forward power at low vacuum levels would be strongly mitigated in high vacuum, where the behaviour is conjectured to be similar to that at room pressure. The idea is therefore to exploit tests at room pressure to avoid the conditions that trigger the uncontrolled discharges, in order to have confirmation that stratification and production of larger samples would be possible in the lunar environment, where the same breakdown condition would occur.

In a first set of tests, the probe was moved along single stripes with a bed-tip distance of 1 mm and a forward power of 100 W, using DNA1_V_I powder. Different feed rates were set, ranging from 2.3 mm/min (the lowest feed rate achievable with the CNC system) to 100 mm/min. The results are shown in Fig. 10.

As can be seen, the molten regolith tends to split into separate spherical domains instead of giving a continuous molten strip, with a behaviour similar to molten glass for which high viscosity and high cohesion forces lead to the minimization of the surface/volume ratio. The phenomenon is well-known in the field of powder bed fusion of metals as the “balling” effect [39]. By reducing the feed rate, the dimensions of the molten domains rise and some begin to bond together, but a single solid strip was not obtained so far.

In a second set of tests, the tool paths shown in Fig. 11A were used at different scanning speeds to implement two adjacent stripes. Results are depicted in Fig. 12. As for the single stripes, the size of the individual domains increases as the feed rate decreases, but bonding between the particles is still difficult.

Finally, a layer-wise strategy was implemented to obtain a solid 3D object. The aim was to obtain a quasi-cubic sample. To do that, a zig-zag stripe scan strategy was programmed as shown in Fig. 11B. To ensure better bonding between the subsequent agglomerates the scan vector was rotated by 90° after every layer, so alternating the scan strategy of Fig. 11B and C. The process parameters used for this test were the same of the stripe tests while the feed rate was set to 2.3 mm/min. The layer thickness was set to approximately 1 mm. To deposit new layers of material upon the first one, an amount of powder was placed on the sintered particles and spread in a homogeneous layer using 1 mm thick sheets as spacer. This procedure was repeated for 5 layers. The result is shown in Fig. 13. An almost cubic sample was produced with approximate dimensions of 11x11 × 6.5 mm (x, y, z). The sample appears as an agglomerate of fused particles partially bonded together.

3.4. Design for embarking considerations

The overall research was developed by taking into account technological choices that would in principle enable the transportation and the use on the lunar surface. Although the technological maturity of the system at the end of the research still needs developments, the study allowed to identify strengths and critical aspects of the LMH solution, as well as to point out a roadmap for the system optimization.

For the microwave generator, the one adopted in this study is not suitable for operation under high vacuum. One necessary change would thus be the choice/development of a device specifically optimized for operation under vacuum conditions. A less straightforward alternative would be to envisage a pressurized module in which the actual generator can be housed.

For the CNC system, an even lighter system could be selected to operate in the absence of gravity. Now that the feasibility of layer superimposition has been proven, a more advanced solution is required in order to automatically add layers of powder one on top of the other. A possible solution could be that of a build platform, on which a mechanical roller or blade spreads and smoothes the powder previously provided by a powder hopper. The individual layers are selectively melted/sintered by the localized microwave source before the deposition of a new layer. At the end of the process, the unsintered powder material is recovered.

For the test setup considered in this paper, a liquid-cooled system was used for the microwave generator. Considering the extreme temperature variations on the Moon, operation of the system would only be possible during the lunar night and, in this case, no cooling would be needed.

A compact computer system consisting of a Single-Board Computer (SBC) can be used to control the CNC and microwave generator). The entire system can be powered by continuous current with a potential of 36 V, easily provided by solar panels without needing for power inverters.

4. Conclusions

The consolidated specimens produced at room and low pressure allowed to verify the feasibility of Localized Microwave Heating for the production of parts using regolith simulants and to increase the TRL from 2 to 4. In this context:

- Microwave heating was effective for both simulants, DNA1_V and DNA1_V_I, as it could achieve temperature ranges for sintering or even melting the powder. The addition of ilmenite to increase microwave absorption does not seem to be necessary and resulted in inconstant results. Hence, the method can be expected as fruitful when used with lunar soils collected in different areas of the lunar surface, also where Fe content is relatively low such as in the lunar Highlands. This aspect is, indeed, of relevant importance considering the interest towards the lunar poles and for the south pole in particular as ideal sites for the first installations.
- The pressure value drastically changes the behaviour of the system: at room pressure, hardly any discharges occur, so that a higher power can be set. If the pressure is lowered to 0.01 mbar, very energy-wasting discharges occur, limiting the maximum power to 50 W. Due to the lower power, melting at a sufficient distance between the tip and the bed is not possible and the sintered product sticks to the antenna tip, hindering the possibility to move the probe to obtain 3D objects.
- Experimental trials carried out in air at atmospheric pressure demonstrated the feasibility of the construction of single/composed sintered stripes and, eventually, of multi-layered samples having considerable dimensions. Glassy spheres are produced whose dimensions increase with decreasing scanning speed. Although achieving a continuous strip of material is difficult, layering produces 3D solid samples consisting of agglomerates of molten particles. Therefore, these results indicate the feasibility of the proposed technology.
- The results should also be reproducible under high vacuum conditions due to the consequences of Paschen’s law. This aspect requires further investigation.

Declaration of competing interest

The authors declare that they have no known competing financial interests or personal relationships that could have appeared to influence the work reported in this paper.

Acknowledgments

This research was part of the MICROLITH project (MICROwaves heating for sintering of regoLITH) founded by the European Space Agency, ESTEC Contract Number 4000133458/20/NL/KML/rk. The authors would like to acknowledge Luca Niccolai (Dynaflex s.r.l., Ancona, Italy) and Prof. Antonije Djordjević (School of Electrical Engineering, University of Belgrade, Serbia) for the technical support in the design and production of the antenna.

References

[1] NASA, Artemis, (n.d.). https://www.nasa.gov/specials/artemis/(accessed December 5, 2022).
[2] ESA, Argonaut – European Large Logistics Lander, 2020. https://www.esa.int/Science_Exploration/Human_and_Robotic_Exploration/Exploration/Argonaut_European_Large_Logistics_Lander. (Accessed 5 December 2022).
[3] H.W. Jones, The recent large reduction in space launch cost, in: 48th Int. Conf, . Environ. Syst., 2018, p. 81. https://ttu-ir.tdl.org/handle/2346/74082.
[4] ESA, Lunar Exploration – ESA's Missions, 2017. https://www.esa.int/Education/Teach_with_the_Moon/Lunar_Exploration_ESA_s_missions. (Accessed 5 December 2022).
[5] M. Anand, I.A. Crawford, M. Balat-Pichelin, S. Abanades, W. van Westrenen, G. Péraudeau, R. Jaumann, W. Seboldt, A brief review of chemical and mineralogical resources on the Moon and likely initial in situ resource utilization (ISRU) applications, Planet, Space Sci 74 (2012) 42–48, https://doi.org/10.1016/j.pss.2012.08.012.
[6] T.L. Wilson, K.B. Wilson, Regolith sintering: a solution to lunar dust mitigation?, Lunar Planet. Sci. XXXVI (2005) Part 21, 1422. https://ntrs.nasa.gov/api/citations/20050180751/downloads/20050180751.pdf.
[7] K.W. Farries, P. Visintin, S.T. Smith, P. van Eyk, Sintered or melted regolith for lunar construction: state-of-the-art review and future research directions, Construct. Build. Mater. 296 (2021) 123627, https://doi.org/10.1016/j.conbuildmat.2021.123627.
[8] L. Song, J. Xu, S. Fan, H. Tang, X. Li, J. Liu, X. Duan, Vacuum sintered lunar regolith simulant: pore-forming and thermal conductivity, Ceram. Int. 45 (2019) 3627–3633, https://doi.org/10.1016/j.ceramint.2018.11.023.
[9] A. Goulas, J.G. Binner, D.S. Engstrøm, R.A. Harris, R.J. Friel, Mechanical behaviour of additively manufactured lunar regolith simulant components, Proc. Inst. Mech. Eng. Part L J. Mater. Des. Appl. 233 (2019) 1629–1644, https://doi.org/10.1177/1464420718777932.
[10] Y. Wang, L. Hao, Y. Li, Q. Sun, M. Sun, Y. Huang, Z. Li, D. Tang, Y. Wang, L. Xiao, In-situ utilization of regolith resource and future exploration of additive manufacturing for lunar/martian habitats: a review, Appl. Clay Sci. 229 (2022) 106673, https://doi.org/10.1016/j.clay.2022.106673.
[11] M. Fateri, A. Meurisse, M. Sperl, D. Urbina, H.K. Madakashira, S. Govindaraj, J. Gancet, B. Imhof, W. Hoheneder, R. Waclavicek, C. Preisinger, E. Podreka, M. P. Mohamed, P. Weiss, Solar sintering for lunar additive manufacturing, J. Aero. Eng. 32 (2019), https://doi.org/10.1061/(ASCE)AS.1943-5525.0001093.
[12] B. Imhof, D. Urbina, P. Weiss, M. Sperl, W. Hoheneder, R. Waclavicek, H. Madakashira, J. Salini, S. Govindaraj, J. Gancet, M. Makthoum, T. Gobert, M. Fateri, A. Meurisse, O. D'Angelo, C. Preisinger, Advancing solar sintering for building A base on the moon, in: 68th Int. Astronaut. Congr. 2017 - 25-29 Sept. 2017, Adelaide, Aust., Adelaide, Australia, 2017.
[13] J. Cheng, D. Agrawal, Y. Zhang, R. Roy, Microwave sintering of transparent alumina, Mater. Lett. 56 (2002) 587–592, https://doi.org/10.1016/S0167-577X(02)00557-8.
[14] K.H. Brosnan, G.L. Messing, D.K. Agrawal, Microwave sintering of alumina at 2.45 GHz, J. Am. Ceram. Soc. 86 (2003) 1307–1312, https://doi.org/10.1111/j.1151-2916.2003.tb03467.x.
[15] A. Borrell, M.D. Salvador, Advanced ceramic materials sintered by microwave technology, in: Sinter. Technol. - Method Appl., InTech, 2018, https://doi.org/10.5772/intechopen.78831.
[16] K. Saitou, Microwave sintering of iron, cobalt, nickel, copper and stainless steel powders, Scr. Mater. 54 (2006) 875–879, https://doi.org/10.1016/j.scriptamat.2005.11.006.
[17] D. Agrawal, Microwave sintering of metal powders, in: Adv. Powder Metall., Elsevier, 2013, pp. 361–379, https://doi.org/10.1533/9780857098900.3.361.
[18] M. Oghbaei, O. Mirzaee, Microwave versus conventional sintering: a review of fundamentals, advantages and applications, J. Alloys Compd. 494 (2010) 175–189, https://doi.org/10.1016/j.jallcom.2010.01.068.
[19] Y. Meir, E. Jerby, Localized rapid heating by low-power solid-state microwave drill, IEEE Trans. Microw. Theor. Tech. 60 (2012) 2665–2672, https://doi.org/10.1109/TMTT.2012.2198233.
[20] M. Salehi, S. Maleksaeedi, M.L.S. Nai, M. Gupta, Towards additive manufacturing of magnesium alloys through integration of binderless 3D printing and rapid microwave sintering, Addit. Manuf. 29 (2019) 100790, https://doi.org/10.1016/j.addma.2019.100790.
[21] H. Curto, A. Thuault, F. Jean, M. Violier, V. Dupont, J.-C. Hornez, A. Leriche, Coupling additive manufacturing and microwave sintering: a fast processing route of alumina ceramics, J. Eur. Ceram. Soc. 40 (2020) 2548–2554, https://doi.org/10.1016/j.jeurceramsoc.2019.11.009.
[22] X. Zhou, P.D. Pedrow, Z. Tang, S. Bohnet, S.S. Sablani, J. Tang, Heating performance of microwave ovens powered by magnetron and solid-state generators, Innov. Food Sci. Emerg. Technol. 83 (2023) 103240, https://doi.org/10.1016/j.ifset.2022.103240.
[23] A. Toossi, H. Moghadas, M. Shayegh, D. Sameoto, M. Daneshmand, Efficient microwave susceptor design for localized heating on substrate, IEEE Trans. Components, Packag. Manuf. Technol. 5 (2015) 570–578, https://doi.org/10.1109/TCPMT.2015.2409791.
[24] L. Thiébaut, A. Cowley, Microwave processing of regolith – a 1D-printing cavity for enabling lunar construction technology, in: In: 8th Eur. Conf. Aeronaut. Sp. Sci. (EUCASS), 1-4 July 2019 - Madrid, 2019, https://doi.org/10.13009/EUCASS2019-917.
[25] L. Sibille, P. Carpenter, R. Schlagheck, R.A. French, Lunar Regolith Simulant Materials: Recommendations for Standardization, Production, and Usage, 2006. NASA/TP-2006-214605.
[26] P. Carpenter, L. Sibille, S. Wilson, G. Meeker, Development of standardized lunar regolith simulant materials, Microsc. Microanal. 12 (2006) 886–887, https://doi.org/10.1017/S143192760606301X.
[27] G. Cesaretti, E. Dini, X. De Kestelier, V. Colla, L. Pambaguian, Building components for an outpost on the Lunar soil by means of a novel 3D printing technology, Acta Astronaut. 93 (2014) 430–450, https://doi.org/10.1016/j.actaastro.2013.07.034.
[28] D.S. McKay, J.L. Carter, W.W. Boles, C.C. Allen, J.H. Allton, JSC-1: a new lunar soil simulant, Eng. Constr. Oper. Sp. IV. 2 (1994) 857–866. https://www.lpi.usra.edu/lunar/strategies/jsc_lunar_simulant.pdf?q=jsc.
[29] J.J. Papike, S.B. Simon, J.C. Laul, The lunar regolith: chemistry, mineralogy, and petrology, Rev. Geophys. 20 (1982) 761–826, https://doi.org/10.1029/RG020i004p00761.
[30] S. Lim, V.L. Prabhu, M. Anand, L.A. Taylor, Extra-terrestrial construction processes – advancements, opportunities and challenges, Adv. Sp. Res. 60 (2017) 1413–1429, https://doi.org/10.1016/j.asr.2017.06.038.
[31] L.A. Taylor, A. Patchen, D.-H.S. Taylor, J.G. Chambers, D.S. McKay, X-ray digital imaging petrography of lunar mare soils: modal analyses of minerals and glasses, Icarus 124 (1996) 500–512, https://doi.org/10.1006/icar.1996.0226.
[32] R.V. Morris, Surface exposure indices of lunar soils - a comparative FMR study, in: Lunar Sci. Conf. 7th, Houston, Tex., March 15-19, 1976, Proc., Pergamon Press Inc., Houston, 1976. https://adsabs.harvard.edu/full/1976LPSC, 7..315M.
[33] T. Häfner, A Microwave Sinter System for Lunar Regolith Studies, Luleå University of Technology, 2016. https://ltu.diva-portal.org/smash/record.jsf?pid=diva2%3A1032476&dswid=1355.
[34] D.R. Williams, Moon Fact Sheet, Nasa, vols. 1–3, 2020. https://nssdc.gsfc.nasa.gov/planetary/factsheet/moonfact.html. (Accessed 9 October 2023).
[35] N. Marquardt, Introduction to the principles of vacuum physics, in: CAS - Cern Accel. Sch. Vac. Technol. 28 May - 3 Jun 1999, Snekersten, Denmark, 1999, pp. 1–24, https://doi.org/10.5170/CERN-1999-005.1.
[36] GRBL, (n.d.). https://github.com/gnea/grbl (accessed January 31, 2024).
[37] P.A. Sohi, M. Kahrizi, Advances in gas ionization sensors based on nanostructured materials: a review, J. Mater. Sci. Mater. Electron. 30 (2019) 19087–19099, https://doi.org/10.1007/s10854-019-02331-8.
[38] W.H. Walton, Feret's statistical diameter as a measure of particle size, Nature 162 (1948) 329–330.
[39] V. Lindström, G. Lupo, J. Yang, V. Turlo, C. Leinenbach, A simple scaling model for balling defect formation during laser powder bed fusion, Addit. Manuf. 63 (2023) 103431, https://doi.org/10.1016/j.addma.2023.103431.